International Journal of Nanomedicine

Dovepress
open access to scientific and medical research

Open Access Full Text Article

ORIGINAL RESEARCH

RETRACTED ARTICLE: IR-enhanced photothermal therapeutic effect of graphene magnetite nanocomposite on human liver cancer HepG2 cell model

Taher A Salaheldin[1,2]
Samah A Loutfy[3]
Marwa A Ramadan[4]
Tareq Youssef[4]
Shaker A Mousa[1]

[1]Pharmaceutical Research Institute, Albany College of Pharmacy and Health Sciences, Rensselaer, NY, USA; [2]Nanotechnology and Advanced Materials Central Lab, Agricultural Research Center, Giza, Egypt; [3]Virology and Immunology Unit, Cancer Biology Department, National Cancer Institute, Cairo University, Cairo, Egypt; [4]Department of Photochemistry Photobiology, National Institute for Laser Enhanced Science (NILES) Cairo University, Cairo, Egypt

Background: Graphene magnetite nanocomposites (G/Fe_3O_4) exhibit light photothermal conversion upon enhancement by 808 nm IR laser excitation. We evaluated the cytotoxic and photothermal effects of G/Fe_3O_4 on a HepG2 human liver cancer cell model.

Methods: Graphene nanosheets (rGO), magnetite nanoparticles (Fe_3O_4), and G/Fe_3O_4 were prepared by chemical methods and characterized using transmission electron microscopy, Raman spectroscopy, zeta analysis, and vibrating sample magnemeter. Dark and light cytotoxicity were screened with colorimetric Sulforhodamine B cell viability assay after 24 and 48 hours. DNA fragmentation and some apoptotic genes on a transcriptional RNA level expression were performed. All prepared nanomaterials were evaluated for their photothermal effect at concentrations of 10 and 50 µg/mL. The power density incident on the cells by 300 mW 808 IR diode laser was 0.597 W/cm^2.

Results: Treatment of HepG2 with 400 µg/mL of rGO, Fe_3O_4, and G/Fe_3O_4 showed alteration in cell morphology after 24 hours of cell treatment and revealed toxic effects on cellular DNA. Evaluation of the cytotoxic effects showed messenger RNA (mRNA) in *β-actin* and *Bax* apoptotic genes, but no expression of mRNA of *caspase-3* after 24 hours of cell exposure, suggesting the involvement of an intrinsic apoptotic caspase-independent pathway. A photothermal effect was observed for G/Fe_3O_4 after irradiation of the HepG2 cells. A marked decrease was found in cell viability when treated with 10 and 50 µg/mL G/Fe_3O_4 from 40% to 5% after 48 hours of cell treatment.

Conclusion: Results indicate that G/Fe_3O_4 nanocomposite was effective at transformation of light into heat and is a promising candidate for cancer therapy.

Keywords: graphene magnetite nanocomposite, HepG2 human liver cancer, cytotoxicity, photothermal effect, PCR

Plain language summary

Cancer is the most challenging fatal disease facing humans in the 21st century. Hundreds of scientific groups, universities, and pharmaceutical companies collectively spend billions of dollars to discover and develop effective drugs. Chemotherapy, the term used to refer to approved drugs administered to patients, is a common cancer treatment although it can have highly toxic side effects. This research used a biocompatible nanomaterial (materials on the scale of 0.000000001 meter) as a new chemotherapy with fewer side effects. Graphene is a carbon sheet loaded with iron nanoparticles forming what is called graphene/iron composite. Both carbon and iron are biocompatible with the human body. Graphene/iron composite is used here for treatment of a liver cancer cell culture model. Efficiency of such materials can be attributed to: 1. its nano size allows it to be at low concentration in a solution but still

Correspondence: Shaker A Mousa
Pharmaceutical Research Institute, Albany College of Pharmacy and Health Sciences, 1 Discovery Drive (Room 238), Rensselaer, NY 12144, USA
Tel +1 518 694 7397
Email shaker.mousa@acphs.edu

http://doi.org/10.2147/IJN.S196256

have a high surface area for nanoparticles to bind to, which aids with high efficiency and fewer side effects, 2. its nano size facilitates the graphene/iron composite's entry inside cancer cells so it effectively "targets" cancer cells, 3. it can be used as a carrier of other drugs to produce a drug-combination treatment, 4. graphene/iron composite exhibits new properties that enable it to absorb infrared light, resulting in heating cancer cells and killing them without harmful effects as compared to traditional chemotherapy, and 5. such treatment is cheap and feasible for application. Our promising results in this study may give new hope for millions of people suffering from cancer.

Introduction

Graphene nanomaterials are materials that are being investigated today, with exciting potential because of their different applications. Besides pure graphene and graphene oxide (GO), graphene-metallic nanocomposites have been synthesized by integrating various types of nanoparticles with graphene or GO nanosheets. Graphene nanocomposites have been widely explored and showed great applications in environmental,[1,2] energy,[3] nanocatalysis,[4] and electrochemistry.[5] Graphene/metallic nanocomposite has strong optical absorption in the near-infrared (NIR) range and is used in photothermal therapy of tumors in experimental animal models.[6–8] Unlike m carbon-based nanomaterials, biomedical applications of gra phene have grown rapidly and exhibit potenti for the future.[9,10] Our previous report showed that the c toxic ffect of GO was at a concentration of 400 µg/mL HepG2 man liver cancer cells as confirmed with flow ytom and DNA fragmentation.[11]

A promising example among ese na composite materials is graphene magnetite n ocomposite (Fe_3O_4), which has been synthesized by s veral gr ups and used for a variety of purposes[12,13] such as drug c ier and as contrast agent for *T2*-weighted mag tic res nce im ing (MRI) and for in vitro cell la ing. I spite in h esearch to determine the biomedical pplicati of many types of graphene-based nanocomposite ost materials studied were less well-functionalized (eg biocompatibility of coating) and thus might not be ideal to e applicable in biological systems.[4]

Photothermal therapy (PTT) has attracted great attention as a safe therapeutic approach in cancer treatment, compared to chemotherapy. Light-absorbing agents are employed to induce photothermal damage of tumor cells after exposure to particular light.[6] Such photothermal effects are exhibited by various nanostructures, carbon nanotubes, and graphene, which are under investigation for their photothermal effects as promising agents for cancer therapy.[7–9]

In such context, the current study focused on evaluating the in vitro cytotoxic and photothermal effects of the prepared nanomaterials in the HepG2 liver cancer cell model. This may open a gate to develop novel nanomaterials with desirable physicochemical properties that can be utilized as a new therapeutic approach against hepatocellular cancer.

Material and methods

Synthesis of graphene oxide (GO)

GO was prepared using modified Hummers method.[14,15] Graphite (0.5 g) (99.9995%, Alfa A ar, rd Hill, MA, USA) was dissolved in 25 mL of s furic acid (9 %, H_2SO_4, Sigma-Aldrich, St. Louis, MO, US and 0.5 g f sodium nitrate (99.9%, $NaNO_3$, Si na-Aldrich was ded to the solution under stirring 15 mi tes. Th eaction vessel was transferred to an ice ba and the temp rature was adjusted below 10°C. The potassium rman nate (99.9%, $KMnO_4$, Sigma-Aldrich) wa lowly adde g over 10 minutes. To get homogenous GO, the mperature must not be elevated over 10°C uring the addition f $KMNO_4$. The reaction mixture was tirred at 35°C overnight. Fifty mL of deionized water was lowly added and the temperature of the reaction was elevate to be r ar 90°C under stirring for 1 hour. Finally, mL of warm deionized water was added, and then 5 mL of h roge peroxide (H_2O_2, 36%, Alfa Aesar) was added. Brownish yellow GO was formed. Dry GO was obtained om three washing cycles using water and centrifugation at 1000 x *g* for 30 minutes then dried at 60°C. Exfoliation of GO was done with sonication (200 w) in deionized water for 1 hour, generating well dispersed GO.

Synthesis of reduced graphene oxide (rGO) nanosheets

Reduction of graphene oxide to graphene is one of the most important transformation processes that can be achieved by using one of several techniques such as thermal, electrochemical, or simply using string reducing agents. Pristine-like graphene sheets have been given a variety of names, including reduced graphene oxide (rGO), chemically-reduced graphene oxide (CReGO), or simply graphene. Graphene can be conjugated with a wide range of nanomaterials to form graphene nanocomposites with potential applications.[13]

In this work, rGO nanosheets were prepared by using chemical reduction of GO. Ascorbic acid (99.9995% Sigma-Aldrich) was used as a biocompatible reducing agent. Typically, 50 mL of the previously prepared GO and

0.1 M ascorbic acid were mixed in a volume ratio of 1:1 and sonicated for 30 minutes at 60°C, and a black suspension formed. The solution was centrifuged at 5000 x *g* to remove the supernatant, and 5 mL of 30% H_2O_2 was added under sonication for 30 minutes at 60°C. After ultrasonication, the resulting graphene sheets were collected by centrifugation at 5000 x *g*, washed with ethanol and water three times and dried at 120°C in a vacuum oven for further characterization.[13]

Synthesis of magnetite nanoparticles (Fe_3O_4) coated with poly ethylene glycol (PEG)

Magnetite nanoparticles (Fe_3O_4) can be prepared in a number of ways, the most common of which is the chemical co-precipitation of Fe salts with the addition of a hydroxide base, allowing the preparation of Fe_3O_4 nanoparticles in a simple way with precise control of size and shape as appropriate for biomedical applications. Mechanistically, monodispersive particles can be obtained via homogeneous precipitation reactions that involve the separation of the nucleation and growth of new nuclei. For our synthesis, the co-precipitation procedure was performed with a dispersant. In a homogeneous precipitation, when the concentration of constituent species reaches critical super-saturation, a short single burst of nucleation occurs. Nuclei are allowed to grow uniformly by diffusion of solutes from the solution to their surface until the final size is reached. The process of precipitation was carried out at pH=10 and can be represented by the following equation:

$$Fe[H_2O]_6^{2+} + Fe[H_2O]_6^{3+} + NaOH = Fe(OH)_2 + Fe(OH)_3 \rightarrow Fe_3O_4$$

Colloidal stability can be achieved by introducing polymeric steric hindrance using PEG polymer coating. It is known that PEG adsorbs non-specifically on oxide surfaces. The interaction with the surface results from hydrogen bonding between polar functional groups of the polymer and the hydroxylated and protonated surface of the oxide.

For our synthesis, the co-precipitation procedure was performed with a dispersant. Magnetite nanoparticles were prepared using 100 mL of 3% PEG (Sigma-Aldrich, MW =8000) solution using deionized water. The PEG solution was bubbled with nitrogen gas for 30 minutes. Then 1.654 g iron (III) chloride anhydrous (Sigma-Aldrich, MW=162.21) and 2 g ammonium iron (II) sulfate hexa hydrate (Sigma-Aldrich) were dissolved in the PEG solution with mechanical stirring. Three M NaOH (Alfa Aesar) was added dropwise into the above mixture under the protection of nitrogen gas with vigorous stirring. An initial brown precipitate formed and turned to black. Once the pH reached 10, stirring was stopped, and the magnetite nanoparticles settled gradually and were collected using an external magnet. Magnetite nanoparticles were washed with deionized water several times and dried in a vacuum oven for further characterization.[16]

Synthesis of graphene/magnetite nanocomposite (G/Fe_3O_4)

The surface of GO is highly rich with oxygen containing groups such as hydroxyl (-OH) and carboxylic (-COOH) that serve as anchoring and active sites for nucleation and growth of magnetite nanoparticles on its surface. A solvothermal method was used to reduce GO to graphene and in situ conversion of Fe^{3+} ions to spherical magnetite nanoparticles simultaneously thus resulting in formation of graphene/magnetite (G/Fe_3O_4) nanocomposites.[1]

In a typical synthesis using the solvothermal method, 0.5 g of the prepared GO was exfoliated with ultrasonication in 80 mL of ethylene glycol (99.999% Sigma-Aldrich) for 1 hour at 40°C. Then, 1.6 g of ferric chloride (Sigma-Aldrich, MW=162.21) and 3.2 g sodium acetate (Alfa Aesar) were added with stirring at room temperature. The mixture was transferred into a Teflon-lined stainless-steel autoclave and kept at 200°C for 6 hours, then left to cool to ambient temperature for 24 hours at room temperature. The black precipitate of G/Fe_3O_4 nanocomposite was formed, and it was centrifuged and washed three times with deionized water to remove unreacted reactants, then finally dried at 60°C in a vacuum oven to prevent the oxidation of magnetite nanoparticles.[1]

Characterization of rGO, Fe_3O_4, and G/Fe_3O_4

Spectral absorption was measured using a double beam UV-Vis-NIR spectrophotometer (Cary 5000, Agilent Technologies, Santa Clara, CA, USA). Morphology was imaged using a High Resolution Transmission electron Microscope (HRTEM, Tecnai, G20, FEI, Almelo, the Netherlands), operating at an accelerating voltage of 200 kV. Drops of dilute prepared nanomaterial solutions were deposited on carbon-coated copper grid and left to dry at room temperature. Raman analysis was performed on a confocal dispersive Raman microscope (DXR 2, Thermo Fisher Scientific, Waltham, MA, USA). Raman scattering was excited with 632.81 nm excitation wavelength supplied by an internal He–Ne laser. Patterns were recorded in the 50–1800 cm^{-1} Raman shift range with

a spectral resolution of 0.5 cm^{-1}. Particle size distribution and electrokinetic potential (zeta potential) were measured with a particle size analyzer (Nano ZS, Malvern Instruments, Malvern, UK) based on a dynamic light scattering technique and electrophoretic light scattering techniques, respectively. Phase analysis was determined with X-ray diffraction (XRD) technique (X'pert PRO, PANanalytical, Almelo, the Netherlands) in the scanning mode operated at 40 kV and a current of 30 mA with Cu K radiation (=1.54 A) and HighScore Plus software. The diffraction intensities were compared with the standard International Centre for Diffraction Data (ICDD) library. The Powder Diffraction File (PDF-4) database was the source for the information regarding the crystal structure of the synthesized nanomaterials. The magnetic properties were measured using a vibrating sample manometer (VSM, Lake Shore Cryotronics, Inc., Westerville, OH, USA).

Cell culture

HepG2 cell line human liver hepatocellular carcinoma (HepG2) was the in vitro model used in the present study. The cells were obtained commercially from a biological products and vaccines company, www.vacsera.com, Cairo, Egypt. The composition of culture and maintenance media (all from Biowest, Nuaillé, France) was RPMI 1640 media, 10% fetal bovine serum, 100 IU/mL 2% penicillin-streptomycin, and 0.5% fungizone. Cells were maintained for 24 hours in monolayer culture at 37°C and 5% CO_2. Then the cells were subcultured using 0.025% trypsin in 0.0025% EDTA (Biowest). To maintain uniformity of cell properties throughout the study, cells were maintained with cryogenic banking of low passage cells. Cell count and viability were monitored with standard Trypan blue dye exclusion procedures. The growth curves for HepG2 cell line were evaluated under baseline conditions prior to investigation of cytotoxicity.[17]

Cytotoxicity assay

Serial dilutions of the prepared nanomaterials were done in 2% RPMI 1640 media, giving concentrations of 125, 250, 500, and 1000 µg/mL. Cytotoxicity was evaluated using Sulforhodamine B (SRB) assay after 24 and 48 hours of cell treatment. All tested runs included negative and positive controls where negative controls were untreated cells subjected to culture media only and were considered as 100% viability. Positive controls were treated with distilled water to be subjected to osmotic shock and were considered as zero viability. Optical density (OD) of positive control was used to subtract background from all treatments. Cellular morphological alterations were examined with phase contrast imaging under 40x objective. The viability percent was estimated using the following equation:

$$\%\text{Viability} = \frac{\text{Mean OD of test sample}}{\text{Mean OD of negative control}} \times 100$$

Cellular uptake of nanomaterials

HepG2 cells were treated with the 400 µg/mL rGO, Fe_3O_4, and G/Fe_3O_4 nanocomposite and incubated for 24 hours, then washed with PBS buffer and fixed with 2% glutaraldehyde for 2 hours. Next they were washed twice with PBS before final fixation in 1% osmium tetroxide for 1 hour. After agarose (1.5%) embedding, Spurr's resin embedding, and ultrathin (50 nm) sectioning, samples were stained with 2% aqueous uranyl acetate and 25 mg/mL lead citrate. Samples were imaged with a Transmission Electron Microscope (Tecnai, G20, Thermo Fisher Scientific, Eindhoven, the Netherlands).[18]

DNA fragmentation

Cellular DNA fragmentation was done following treatment of HepG2 cells with a concentration of twice the IC50, for 24 hours. Then, 100 ng of extracted cellular DNA (Genomic DNA Purification Kit, Amersham Biosciences, Promega, Leiden, the Netherlands) was subjected to 1.5% agarose gel electrophoresis in Tris-acetate buffer pH (8.2) and stained with 0.5 µg/mL ethidium bromide. DNA fragment bands were examined under UV trans-illumination and photographed. It is well known that smearing, or presence of many low molecular weight DNA fragments, is an indication of apoptotic cells.[17,19]

Apoptotic genes detection

One-step reverse-transcription polymerase chain reaction (RT-PCR) assay was used to evaluate the cytotoxic effect of the tested nanomaterials on the expression of selected apoptotic genes, namely *β-actin, Bax*, and *caspase-3* at the transcriptional level. The test was performed after treatment of HepG2 with rGO, Fe_3O_4, and G/Fe_3O_4 at a concentration that was double the IC50, for 24 hours. The *β-actin* housekeeping gene was determined in each run to ensure RNA integrity. The detection of mRNA was previously optimized at different annealing temperatures.[20]

Light toxicity assay

The in vitro light cytotoxicity was measured using SRB assay that was carried out to determine the cell viabilities relative to the control unexposed cells. HepG2 cells were seeded into 96-well cell-culture plates and then incubated for 48 hours at 37°C and 5% CO_2. Then HepG2 cells were exposed to 808 nm optical fiber-coupled diode NIR laser at a power of 300 mW used to irradiate cells at a power density of 0.597 W/cm^2 for different time exposure periods.

Photothermal activity

In this experiment, HepG2 cells were incubated with different concentrations (10, 50 µg/mL) of graphene, GO, graphene/magnetite composite and magnetite for 24 and 48 hours (these concentrations were nontoxic when tested in a dark toxicity test), then an 808 nm diode NIR laser with maximum power 300 mW was used to irradiate cells at a power density of 0.597 W/cm^2 for different time exposure periods (2, 4, 6, 8, 10, 12, 14 and 16 minutes). A standard colorimetric assay using SRB was conducted to screen the cytotoxic effect of our prepared nanomaterials after photothermal ablation.

Results and discussion

Characterization of rGO, Fe_3O_4 and G/Fe_3O_4 nanomaterials

Figure 1A shows a broad diffraction peak at about 2θ=24.20, which could be attributed to the (0 0 2) reflection plane of the graphene nanosheets, confirming that GO has been reduced to graphene (rGO) successfully. The X-ray diffraction (XRD) pattern in Figure 1B illustrates that magnetite was formed in highly purified and crystalline form known by its narrow and intense characteristic peak at 2θ=35.2° (3 1 1). Figure 1C represents the XRD patterns of graphene/magnetite nanocomposite, showing characteristic peaks at 2θ values of 18.3° (1 1 1), 30.1° (2 2 0), 35.5° (3 1 1), 43.1° (4 0 0), 53.6° (4 2 2), 57.0° (5 1 1), and 62.5° (4 4 0). These are consistent with the standard XRD data for the cubic phase Fe_3O_4 with face-centered.

The transmission electron microscopy (TEM) image in Figure 2A shows some deformation and distortion of the graphene nanosheets after the reduction process. A representative TEM micrograph of polymer-coated magnetite nanoparticles is shown in Figure 2B. The results suggest that there is a size limit above which particles will sediment and below which particles will remain suspended

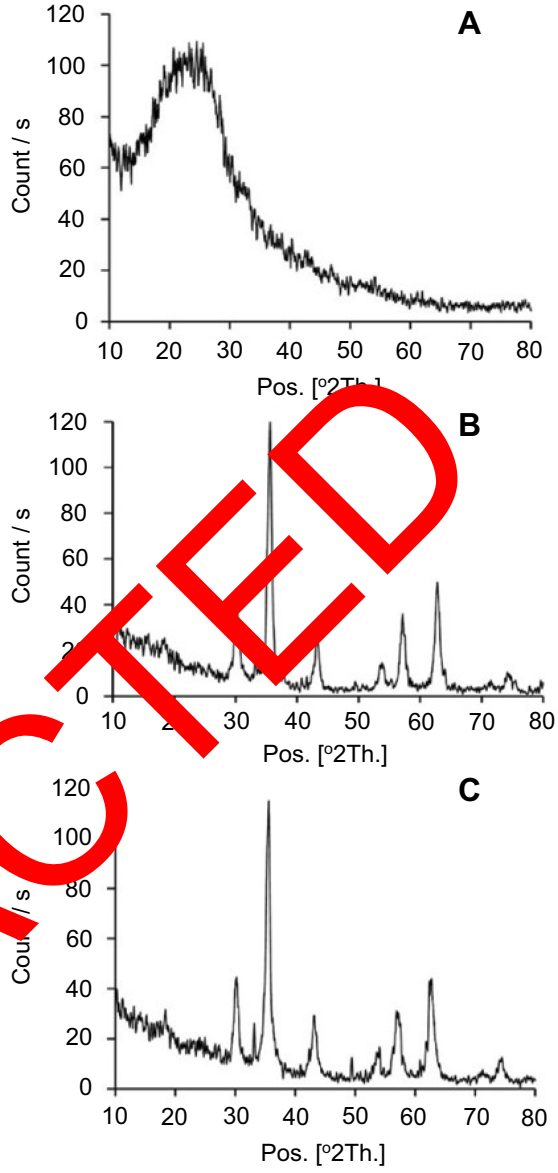

Figure 1 X-ray diffraction (XRD) patterns of (**A**) graphene nanosheets rGO, (**B**) magnetite nanoparticles Fe_3O_4, (**C**) graphene/magnetite nanocomposite G/Fe_3O_4.

indefinitely; the size is dependent on the density of the colloidal material and is ~10 nm for magnetite (Fe_3O_4) particles, with a density of 5.2 g/cm. Figure 2C shows HRTEM imaging of the Fe_3O_4, indicating production of a large quantity of nearly uniform monodispersed spheres. After the combination with the graphene to form the G/Fe_3O_4 nanocomposite, the Fe_3O_4 spheres are uniformly decorated and firmly anchored on the wrinkled graphene layers with a high density and serve as a stabilizer for separate graphene sheets against the aggregation.[1]

We note that the solvothermal reduction was the best method because significant change in morphology can be observed on the obtained graphene sheets, which displayed

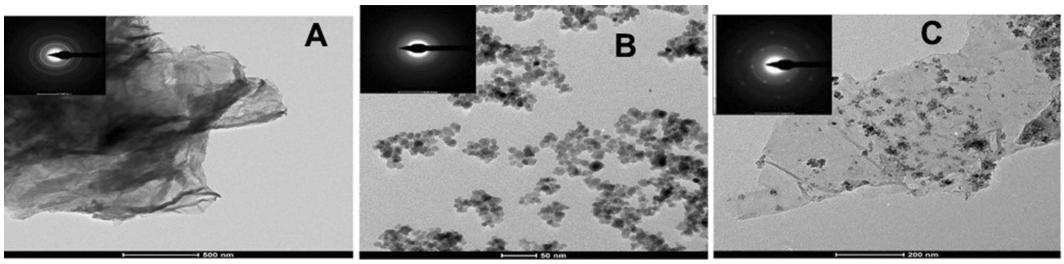

Figure 2 TEM images and diffraction pattern of (**A**) graphene nanosheets rGO (magnification 500 nm), (**B**) magnetite nanoparticles Fe_3O_4 (magnification 50 nm), (**C**) graphene magnetite nanocomposite G/Fe_3O_4 (magnification 200 nm).

layered structures and became very thin. The folding nature was clearly visible. The graphene sheets are exfoliated and cannot restack anymore, which is consistent with the result of XRD.

Raman spectroscopy has proved to be well suited to the molecular morphology characterization of carbon nanomaterials. It is known that every band in the Raman spectrum corresponds directly to a specific vibrational frequency of a bond within the molecule, and such vibrational frequency and hence the position of the band is sensitive to the orientation of the bands and weight of the atoms at either end of the bond. Raman microscopy couples a Raman spectrometer to a standard optical microscope, allowing high magnification visualization of graphene and Raman analysis with a microscopic laser spot.[21] Raman spectra of the GO sample (Figure 3A) showed two distinct peaks at about 1355 cm^{-1} and 1593 cm^{-1} corresponding to the well-documented D and G bands, respectively. The G band originates from in-plane stretching vibrations of sp2 carbon atoms in both rings and chains. Even at low intensity, the D mode can be observed in the Raman spectrum of graphene and is due to the breathing modes of sp2 carbon atoms in rings. Generally, the D mode is

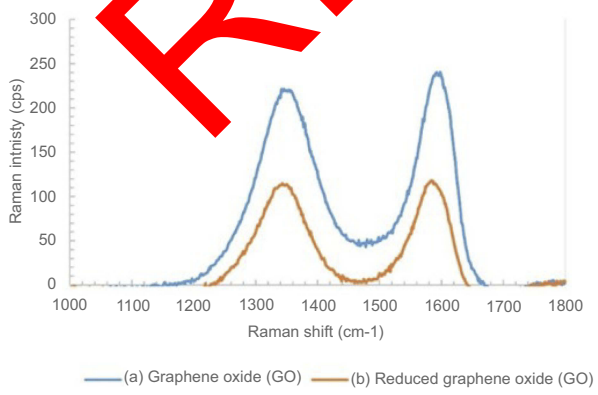

Figure 3 Raman spectra of (**A**) graphene oxide (GO), (**B**) reduced GO (rGO).

associated with the presence of graphene structural defects.[22] So, the strong intensity of the D band for GO indicates the presence of high density defects and structural disorder.[23] In the rGO Raman spectra (Figure 3B), the D band appeared at about 1343 cm^{-1} and the G band at about 1584 cm^{-1} with a red shift indicating the formation of rGO.[22] It was also observed that the G band of GO was much broader than for rGO and was blue-shifted to 1593 cm^{-1}. The D band of GO was also modified, exhibiting a much higher intensity due to the disorder in the sp2 structure induced after the oxidation of graphite and to the attachment of hydroxyl and epoxide groups on the planar carbon structure. The increase of the ratio between the intensities of the D and G bands (ID/IG) is an indication of disorder in carbon material, originating from defects associated with vacancies, grain boundaries, and amorphous carbons.[24] ID/IG was 0.91 and 0.97 for GO and rGO, respectively, indicating disruption of the lattice symmetry and deformation in GO sheet during the hydrothermal reduction process and the formation of rGO.[25]

The successful synthesis of reduced graphene by ascorbic acid was also confirmed with UV-visible spectra of graphene (Figure 4A), which was observed at about 260 nm. Magnetite nanoparticles solution has high background dark color with a broad absorption band visible (Figure 4B). The visible and NIR optical absorbance of graphene/magnetite nanocomposite G/Fe_3O_4 was significantly enhanced compared to pristine GO (Figure 4C) owing to the partial reduction of GO during the formation of magnetite on rGO sheets and indicating that the electronic conjugation within graphene sheets is restored after the reaction.[13]

As shown in Figure 5A, after the reduction of GO nanosheets, the surface of rGO has lowered negative charge, which was clearly observed from zeta potential measurements; the average surface potential was −21.6 mV. The surface of magnetite nanoparticles is mostly negatively charged due to coating with PEG, as clearly observed from

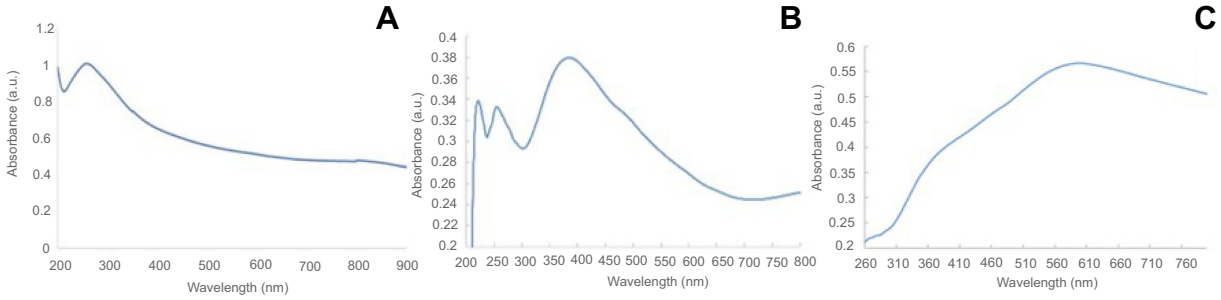

Figure 4 UV-visible absorption curve of (**A**) graphene nanosheets rGO, (**B**) magnetite nanoparticles Fe_3O_4, (**C**) graphene/magnetite nanocomposite G/Fe_3O_4.

zeta potential measurements Figure 5B. The average surface potential was −6 mV, enabling it to form a stable solution in water and facilitate its absorption by cellular membrane. This is related to the small crystallite sizes of magnetite particles that were about 10 nm and have superparamagnetic properties that make them good candidates to be used for cancer therapy and imaging. The surface of graphene/magnetite nanocomposite Figure 5C is mostly negatively charged due

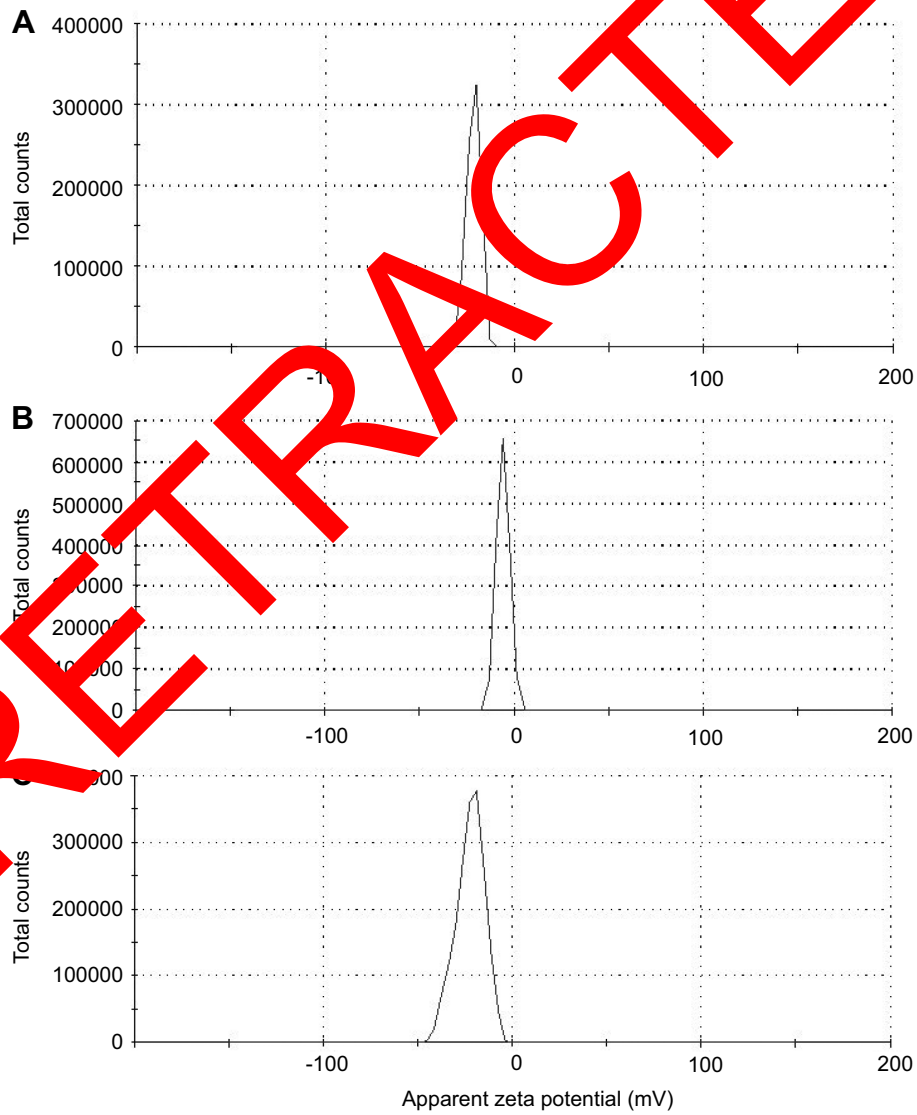

Figure 5 Zeta potential of (**A**) graphene nanosheets rGO, (**B**) magnetite nanoparticles Fe_3O_4, (**C**) graphene/magnetite nanocomposite G/Fe_3O_4.

to coating with PEG that was clearly observed from zeta potential measurements. The average surface potential was −22.2 mV, enabling it to form a stable solution in water and facilitate its absorption by cellular membrane.

A vibrating sample magnetometer (VSM) was used to measure magnetic properties of the prepared magnetite nanoparticles. Magnetic measurements were done at room temperature on an unoriented, random assembly of magnetite nanoparticles for each measurement. A hysteresis loop was generated from which remnant magnetization (Mr), saturation magnetization (Ms), and the intrinsic coercivity (Hc) were measured. Figure 6 shows the magnetic hysteresis loops of the prepared Fe_3O_4 measured with VSM at room temperature (300 K) under an applied magnetic field of 20 kG. Results were Ms of 62.028 emu/g, Hc of 8.5339 G, and Mr was 0.60143 emu/g. Results for G/Fe_3O_4 nanocomposite under the same applied external magnetic field (Figure 6B) were Ms of 45.2 emu/g, Hc was about 14.530 G, and Mr was 0.932 emu/g. These results demonstrate that G/Fe_3O_4 composite exhibits ferromagnetic character with lower Ms than that of the Fe_3O_4 nanoparticles. This reflects the standard practice of normalizing the magnetization by the mass of magnetic constituent.[1] Therefore, the amount of the nonmagnetic graphene sheets compared to the total magnetization might be responsible for such a decrease in Ms.

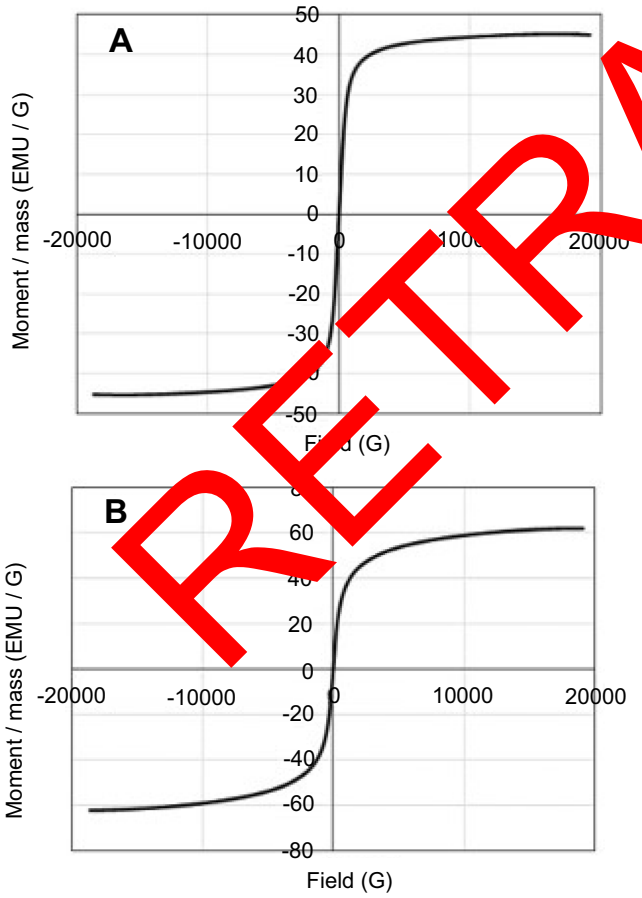

Figure 6 Hysteresis loop for (**A**) magnetite nanoparticles Fe_3O_4, (**B**) graphene/magnetite nanocomposite G/Fe_3O_4.

Interaction of rGO, Fe_3O_4 and G/Fe_3O_4 nanomaterials with HepG2 cells

Previous studies have demonstrated biomedical applications of graphene nanosheets and its composites, especially of their antitumor and antimicrobial activities.[26] The present study used a human HepG2 cell line as an in vitro model to test the anticancer activities of G/Fe_3O_4 nanocomposite and with IR laser enhancement as a new targeted drug for PTT. Traditional treatment approaches are not effective and are subject to eventual therapy resistance in patients. They require invasive procedures, therefore, there is a need for novel treatment approaches to control such incurable disease.

Graphene attached easily to the cell membrane due to presence of large ionic and aromatic groups. Ionic groups such as carboxyl (-COO-) can form electrostatic interactions with cell proteins and DNA. The carboxylic groups are weak ionizable groups that work as low strength acid resins, allowing ion exchange interactions with charged cellular protein molecules, which can be tunable.[27] Previous research has shown that GO may induce in vitro cytotoxicity in cancer cell lines and has emphasized its promising role in cancer therapy.[4,5,7]

Interaction of the prepared nanomaterials with HepG2 cells

Light microscopy

HepG2 cells were treated with 400 µg/mL of the prepared nanomaterials for 24 hours and showed morphological alteration compared to untreated cells (previous work[11]) (Figure S1).

Transmission electron microscopy

HRTEM imaging demonstrated binding and internalization of rGO, Fe_3O_4, and G/Fe_3O_4 into the cultured HepG2 cells. Agglomerations of nanomaterials forming clusters on the cell membrane is evident in the intracellular interaction (Figure 7A–C). Higher magnification images show intracellular clusters, mainly associated with membranes. It was clear that the most accumulated nanoparticles were in cytoplasm. Moreover, it is noted that treatment with nanomaterials was associated with fragmentation and disruption of intracellular organelles with its localization into mitochondria, nucleus, and

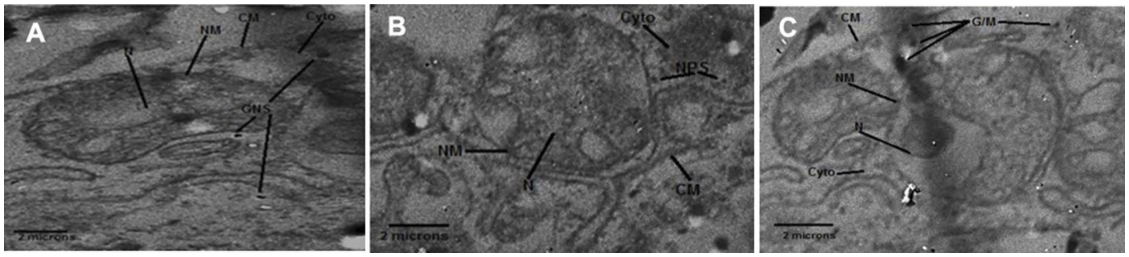

Figure 7 TEM images of HepG2 cell line after incubation for 24 hours with 400 µg/mL of (**A**) graphene nanosheets rGO, (**B**) magnetite nanoparticles Fe_3O_4, (**C**) graphene/magnetite nanocomposite G/Fe_3O_4 with a magnification of 8000x.
Abbreviations: CM, cell membrane; Cyto, cytoplasm; N, nucleus; NM, nuclear membrane; GNS, graphene nanosheets; NPS, magnetite nanoparticles; G/M, graphene/magnetite nanocomposite.

nuclear membrane comparable to untreated cells (data published by our group in previous work[11]).

Dark cytotoxic effect on HepG2

Cellular toxicity of the tested nanomaterials in the absence of light exposure has been evaluated in order to exclude the toxic concentrations in dark reaction and to monitor the selectivity of the applied therapeutic modality. Cytotoxic effect of the prepared nanomaterials was measured using SRB colorimetric assay after treatment of cells with different concentration of the prepared nanomaterials (125, 250, 500 and 1000 µg/mL) for 24 hours. Our results showed that magnetite nanoparticles and graphene magnetite nanocomposite were safe up to a concentration of 1000 µg/mL as shown in Figure 8A. In contrast, cell viability after treatment with graphene was 60% at the same concentration (1000 µg/mL) after the same time of cell treatment (24 hours). Upon extending the length of incubation time to 48 hours using the same concentration of nanomaterials (125, 250, 500 and 1000 µg/mL), our results showed that the viability was decreased, with IC_{50} of 438, 392, and 221 µg/mL for magnetite, graphene, and graphene magnetite, respectively (Figure 8B). Interestingly, the viability of all nanomaterials was 15% for all our nanomaterials at a concentration of 500 µg/mL after 48 hours of cell treatment. This indicates that the effect of nanomaterials on cells is dose- and time-dependent as previously demonstrated.[28]

We previously mentioned that GO caused a dose-dependent decrease in the cell viability because it can penetrate plasma membrane and induce its apoptotic effect. Extending time of treatment to 48 hours leads to a continuous release and uptake of nanoparticles that can disturb the chemical and physiological functions of the cells and therefore decrease the cell viability, a feature that was less obvious after only 24 hours incubation.[11]

DNA fragmentation of all nanomaterials

DNA fragmentation was performed as a characteristic of genotoxic effect and late apoptotic effect. Our results showed that the extracted DNA from cells treated with 400 µg/mL was 204, 132, and 119.8 ng/µL for graphene, graphene magnetite, and magnetite, respectively, compared to 377.2 ng/µL for the untreated cells (cell control) (Table 1 and Figure S2).

Apoptotic genes expression

Housekeeping gene *β-actin* was run in each experiment to ensure an abundant amount of RNA and its intactness and

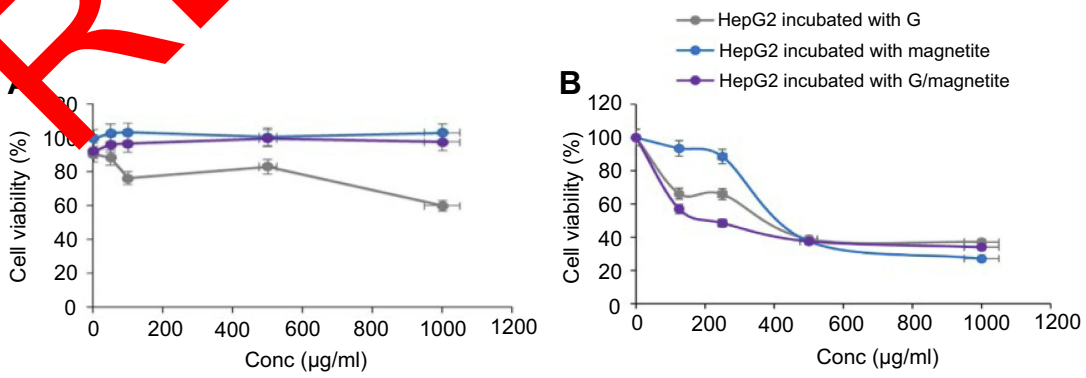

Figure 8 Dark toxicity test at different concentrations (µg/mL) of graphene nanosheets rGO, magnetite nanoparticles Fe_3O_4 and graphene/magnetite nanocomposite G/Fe_3O_4 on HepG2 cells after incubation for (**A**) 24 and (**B**) 48 hours.

Table 1 Genomic DNA content in DNA fragmentation assay before and after treatment of HepG2 with 400 µg/mL nanomaterials

Sample	DNA concentration (ng/µL)	Ratio 260/280
Cells treated with graphene	204	1.95
Cells treated with magnetite	119.8	1.85
Cells treated with graphene/magnetite nanocomposite	132	1.86
Control (untreated cells)	377.2	1.95

to validate our results. Our results showed that *β-actin* was expressed in cells treated with all four prepared nanomaterials and in untreated cells as well, indicating the intactness of mRNA and validity of the extracted RNA.

Regarding expression of mRNA of the apoptotic genes, the expression level of mRNA of *Bax* gene was lower in cells treated with graphene and graphene/magnetite nanocomposite than the cells that were treated with magnetite. But mRNA of caspase-3 was not expressed in cells treated with the nanomaterials, indicating that an intrinsic caspase-independent apoptotic pathway existed with our designed nanomaterials (Figure S3).

In agreement with previous reports, magnetite nanoparticles did not reveal any DNA alteration, even at higher concentrations because Fe_3O_4 nanoparticles weren't able to induce oxidative stress of DNA to cause DNA damage. Similar results were obtained by Hong et al[29] who reported that magnetite nanoparticles did not show any DNA damage in the L-929 fibroblast cell line.[29] In the same track, iron oxide nanoparticles and surface-modified iron oxide nanoparticles induced lower toxicity in L-929 cells.[30]

However, the mechanism by which our nanomaterials exert their cytotoxic effects on biological cells was not thoroughly investigated quantitatively. One of the most commonly suggested cytotoxicity mechanisms is reactive oxygen species (ROS) generation.[31] It has been reported that the interaction of light metal oxide nanoparticles involving magnetite nanoparticles leads to different types of DNA changes such as mutations, DNA strand breakage, chromosomal aberrations, and oxidative DNA damage.[32]

Reports revealed that carbon-based nanostructures, including graphene, induce the cellular apoptotic pathway. There are multiple factors affecting the apoptotic effects induced by carbon nanomaterials – shape, size, cell type, and concentration. For shape, multi-walled carbon nanotubes and nano diamonds can stimulate the expression of chromosomal DNA damage biomarkers including Rad51, p53 and MOGG-1 caused by generation of ROS.[33] For size, the toxic effect of graphene strongly depends on its lateral size where it induced DNA fragmentation caused by oxidative stress and direct contact of the sharp edges with the plasma cell membrane.[34] For cell type, it has been observed that carbon materials except GO showed genotoxicity in U87 glioblastoma cancer cells,[35,36] but daunorubicin/graphene-gold nanocomposites induced apoptosis in multidrug-resistant leukemia cells via activating caspase-3.[37] This indicates that cells behaved differently upon response to different materials, depending on cellular uptake. For concentration, graphene toxicity is concentration-dependent; it stimulates ROS generation and caspase-3 activation in a concentration- and time-dependent manner resulting in induction of apoptosis.[38] Moreover, it is confirmed that ROS can mediate activation of poly ADP-ribose polymerase-1 (PARP-1), and PARP-1 is necessary for mitochondrial release of AIF inducing apoptosis with DNA damage in a caspase-3 independent pathway.[39] In the current study, treatment of HepG2 cells with our nanomaterials could induce apoptosis via caspase-independent pathway or mitochondrial pathways, such as as Bax and Bak, and were activated without the ability to detect caspase-3. This, in turn, causes pores in mitochondria membrane, disrupting it and then leading to release of cytochrome c, which stimulates a cascade of death compounds and ultimately cell death as explained by Pistritto et al.[40] However these results need to be assessed on a protein level to confirm such pathways and to investigate ROS stimulation.[41]

IR photothermal therapy of prepared nanomaterials in HepG2

A control experiment was conducted to evaluate the effect of light source used on HepG2 cell line viability in the absence of the nanomaterials in order to ensure that the previous results were obtained only due to the activation of the nanoparticles by the laser light. Figure 9A shows the effect of NIR laser on the viability of HepG2 cells at different time exposure periods. As seen in the Figure, the laser light has no cytotoxic effect on the cells up to 30 minutes.

The NIR region covers a wavelength range from 650 to 1350 nm and is known as the optical or therapeutic window where light can reach maximum depth of tissue

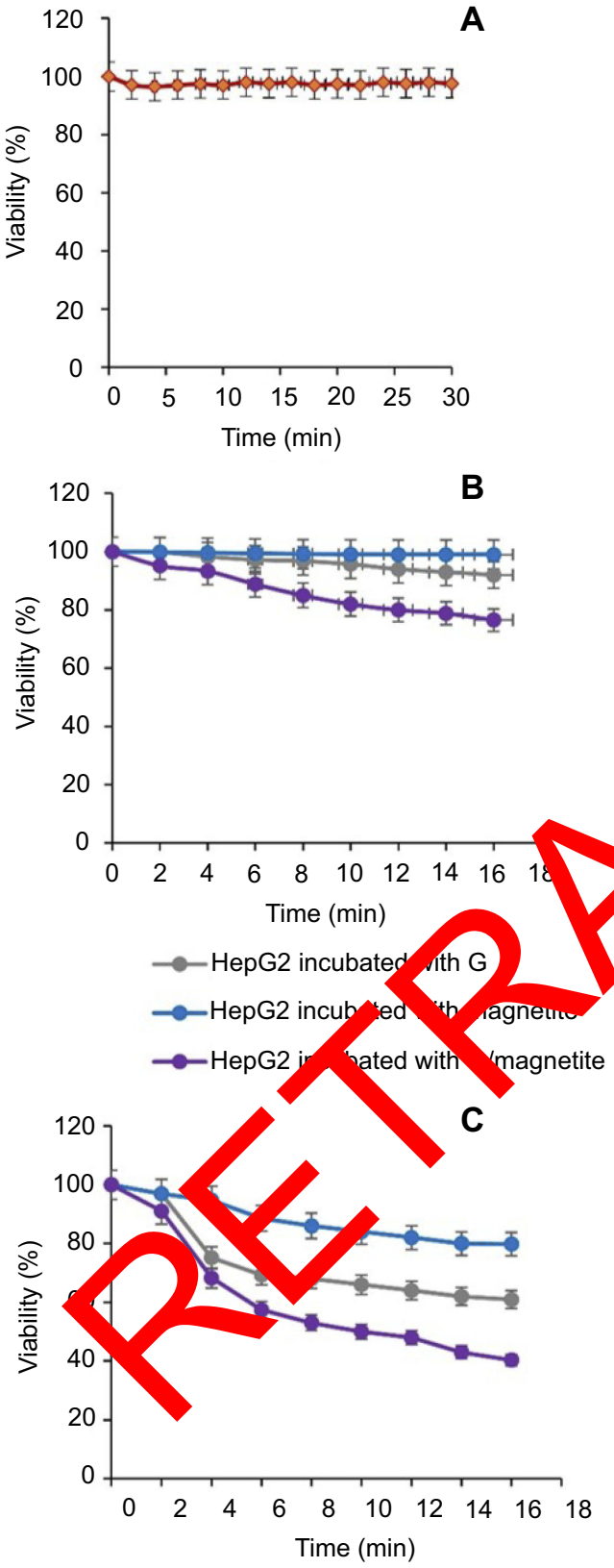

Figure 9 The effect of 300 mW, 808 NIR laser beam on % survival of HepG2 cell line at different exposure times (**A**) in the absence of nanoparticles, (**B**) incubation with 10 μg/mL nanomaterials for 24 hours, and (**C**) incubation with 10 μg/mL nanomaterials for 48 hours.

penetration. In addition, within the NIR region, light scattering is the most dominant light-tissue interaction, and the propagating light becomes diffused rapidly. A scattering phenomenon increases the distance travelled by photons within tissue, so the photon absorption by issue also increases. Scattered light is weakly dependent on wavelength, hence the NIR effect is limited by the light absorption of blood and water at short and long wavelengths, respectively. There are several medical imaging techniques that make use of the NIR window approach such as fluorescence image-guided surgery to detect deep structures.[42] Water doesn't absorb in visible light, it becomes absorbing over the NIR region, and it is a critical component for NIR window applications because its concentration is high in human tissue. Treatment of HepG2 cells with the prepared nanomaterials at a concentration of 10 μg/mL for 24 hours and cell exposure to 0.597 W/cm^2 with an 808 NIR laser beam showed no noticeable decrease in the cell viability by increasing the irradiation time to 16 minutes for rGO and magnetite nanomaterials. In contrast, a marked decrease in the viability was observed after incubation with graphene/magnetite nanocomposite at the same irradiation time (Figure 9B and C).

Upon extending incubation time of the treated cells with all nanomaterials at a concentration of 10 μg/mL to 48 hours and exposing to 0.597 W/cm^2 808 NIR laser beam, results showed that the cell viability decreased by gradually increasing the irradiation time. The percent of cell viability was 79.75%, 60.94% and 40.32% for magnetite, graphene, and graphene/magnetite, respectively (Figure 9B and C). Therefore, the more the exposure light dose, the less the average survival rate. Such decrease in the survival percentage as the exposure light dose increases indicates that the light source has an additional cytotoxic effect on the treated HepG2 cell line with our prepared nanomaterials. Moreover, when treating cells with higher concentration (50 μg/mL) of all nanomaterials and exposing to the same laser beam with analysis after 48 hours of cell treatment, our results showed a marked decrease in the viability of cells treated with G/Fe_3O_4, which decreased to 5.64% after 16 minutes of cell exposure to light (Figure 10). This indicates effective photothermal properties of graphene/magnetite nanocomposite when compared to other prepared nanomaterials. So owing to its strong optical absorption in the NIR window, graphene magnetite

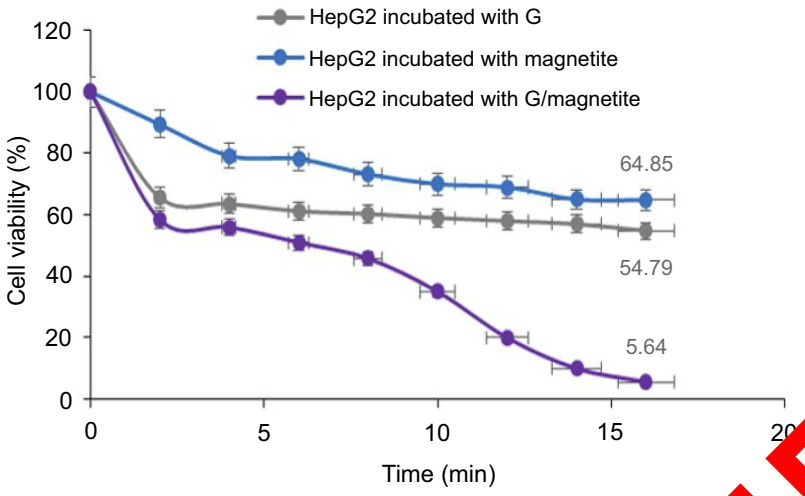

Figure 10 The effect of 300 mW, 808 NIR laser beam on % survival of HepG2 cell line after incubation for 48 hours with 50 µg/mL nanomaterials at different exposure times.

nanocomposite was utilized for photothermal ablation of cancer and can be considered as a promising new material for biological and medical applications.

Conclusion

We succeeded in preparing rGO, Fe_3O_4, and G/Fe_3O_4 nanocomposite, with an excellent stability in water. The resulting composite combined features of Fe_3O_4 and graphene, and thus exhibited the extraordinary advantages of the superparamagnetic and optical properties. The prepared nanomaterials were characterized and studied using XRD, TEM, VSM, UV-Vis-NIR spectroscopy and Zetasizer Nano.

Cytotoxicity evaluation was performed with the SRB colorimetric assay using the HepG2 liver cancer cell line and indicated a mild toxicity (about 40%) at 100 µg/mL of G/Fe_3O_4 nanocomposite, and the toxic effect increased to 62.5% at 400 µg/mL for all the prepared nanomaterials after 48 hours of cell incubation. Results were confirmed by the genotoxic effect observed of all prepared nanomaterials at a concentration of double the IC50 using DNA fragmentation assay. Extensive evaluation of the cytotoxic effect on a molecular level was performed by detecting mRNA expression of some apoptotic genes (*Bax* and *caspase-3*). Our results show lower expression of mRNA of the *Bax* gene in graphene and graphene magnetite with no expression of mRNA of *caspase-3*. This indicates that the apoptosis process is a caspase-independent pathway for all tested nanomaterials, and the generation of ROS by nanoparticles is one of the suggested mechanisms. An increase in the amount of ROS is associated with loss of mitochondrial integrity and activation of the pro-apoptotic Bax, and this may initiate the apoptotic mechanism. This may require investigating apoptotic protein expression to confirm the suggested mechanism.

Regarding the photothermal effects of the G/Fe_3O_4 nanocomposite by irradiation of the HepG2 cells for different exposure times, results showed that treatment of cells with 50 µg/mL of graphene magnetite nanocomposite revealed a marked decrease in the cell viability from 40% to 5%. This indicates that G/Fe_3O_4 nanocomposite was very effective at transformation of light into heat and could be a promising candidate for cancer treatment.

Abbreviations list

GO, graphene oxide; G/Fe_3O_4, graphene magnetite nanocomposite; NIR, near-infrared; rGO, reduced graphene oxide; XRD, X-ray diffraction.

Acknowledgment

There is no funding to report.

Author contributions

All authors contributed to data analysis, drafting or revising the article, gave final approval of the version to be published, and agree to be accountable for all aspects of the work.

Disclosure

The authors report no conflicts of interest in this work.

References

1. Ai L, Zhang C, Chen Z. Removal of methylene blue from aqueous solution by a solvothermal-synthesized graphene/magnetite composite. *J Hazard Mater*. 2011;192(3):1515–1524. doi:10.1016/j.jhazmat.2011.06.068
2. Farghali MA, El-Din TAS, Al-Enizi AM, El Bahnasawy RM. Graphene/magnetite nanocomposite for potential environmental application. *Int J Electrochem Sc*. 2015;10(1):529–537.
3. Dobrota AS, Pasti IA, Mentus SV, Johansson B, Skorodumova NV. Functionalized graphene for sodium battery applications: the DFT insights. *Electrochim Acta*. 2017;250:185–195. doi:10.1016/j.electacta.2017.07.186
4. Yang K, Zhang S, Zhang G, Sun X, Lee ST, Liu Z. Graphene in mice: ultrahigh in vivo tumor uptake and efficient photothermal therapy. *Nano Lett*. 2010;10(9):3318–3323. doi:10.1021/nl1017157
5. Chen W, Yi P, Zhang Y, Zhang L, Deng Z, Zhang Z. Composites of aminodextran-coated Fe_3O_4 nanoparticles and graphene oxide for cellular magnetic resonance imaging. *ACS Appl Mater Interfaces*. 2011;3(10):4085–4091. doi:10.1021/am2009647
6. Robinson JT, Tabakman SM, Liang Y, et al. Ultrasmall reduced graphene oxide with high near-infrared absorbance for photothermal therapy. *J Am Chem Soc*. 2011;133(17):6825–6831. doi:10.1021/ja2010175
7. Ma X, Tao H, Yang K, et al. A functionalized graphene oxide–iron oxide nanocomposite for magnetically targeted drug delivery, photothermal therapy, and magnetic resonance imaging. *Nano Res*. 2012;5:199–212. doi:10.1007/s12274-012-0200-y
8. Huang X, Jain PK, El-Sayed IH, El-Sayed MA. Plasmonic photothermal therapy (PPTT) using gold nanoparticles. *Lasers Med Sci*. 2008;23(3):217–228. doi:10.1007/s10103-007-0470-x
9. Wang S, Zhang Q, Luo XF, et al. Magnetic graphene-based n[illegible]ther-anostic agent for dual-modality mapping guided photothermal [illegible]erapy in regional lymph nodal metastasis of pancreatic cancer. *Biomat[illegible]ials*. 2014;35(35):9473–9483. doi:10.1016/j.biomaterials.2014.07.064
10. Yang K, Hu LL, Ma XX, et al. Multimodal im[illegible]ng g[illegible]ded pho[illegible]-thermal therapy using functionalized graphe[illegible] nanoshe[illegible]s anchor[illegible] with magnetic nanoparticles. *Adv Mater*. [illegible]012;24(1[illegible]1868–1872. doi:10.1002/adma.201104964
11. Loutfy SA, Salaheldin TA, Ramada [illegible]MA, Farro[illegible]XY, Abdallah ZF, Youssef T. Synthesis, characteriz[illegible]nd cytotoxic e[illegible]luation of graphene oxide nanosheets: in vitr[illegible]ver ca[illegible]r model. *Asian Pac J Cancer Prev*. 2017;18(4):955–961. [illegible]i:10.22034/A[illegible]CP.2017.18.4.955
12. Liu X, Tao H, Yang K, Zhang S, Lee ST, [illegible] Z. Optimization of surface chemistry o[illegible]single-wa[illegible]led carbon nanotubes for in vivo photothermal abla[illegible]n of tum[illegible]s. *Biomaterials*. 2011;32(1):144–151. doi:10.1016/j.biomate[illegible]ls.[illegible]10.08.096
13. Zhu X, Liu[illegible]u X, L[illegible] Xu M, [illegible]ang Y. Reduction of graphene oxide vi[illegible]scorbic acid and [illegible]ication for simultaneous detection of d[illegible]amine an[illegible] ascorbic a[illegible]d. *Int J Electrochem Sci*. 2012;7(6):51[illegible]–5184.
14. Hummel[illegible]S, Offeman RE. Preparation of graphitic oxide. *J Am Chem Soc*. [illegible]58;80(6):1339. doi:10.1021/ja01539a017
15. Park S, Ruoff [illegible]Chemical methods for the production of graphenes. *Nat Nanotechnol*. 2009;4(4):17–24. doi:10.1038/nnano.2008.388
16. Răcuciu M, Creangă DE, Bădescu V, Airinei A. Synthesis and physical characterization of magnetic nano-particles functionalized with β-cyclodextrin. *J Optoelectron Adv Mater*. 2007;9:1530–1533.
17. Loutfy SA, Shalaby RH, Hamed AR, et al. Evaluation of cytotoxic effect of metallic nanoparticles in an in vitro liver cancer model. *Chem Pharm Res*. 2015;7:470–487.
18. Zhu ZJ, Ghosh PS, Miranda OR, Vachet RW, Rotello VM. Multiplexed screening of cellular uptake of gold nanoparticles using laser desorption/ionization mass spectrometry. *J Am Chem Soc*. 2008;130:14139–14143. doi:10.1021/ja805392f
19. Loutfy SA, Al-Ansary NA, Abdel-Ghani NT, et al. Anti-proliferative activities of metallic nanoparticles in an in vitro breast cancer model. *Asian Pac J Cancer Prev*. 2015;16(14):6039–6046.
20. Loutfy SA, El-Din HMA, Elberry MH, Allam NG, Hasanin MTM, Abdellah AM. Synthesis, characterization and cytotoxic evaluation of chitosan nanoparticles: in vitro liver cancer model. *Adv Nat Sci-Nanosci Nanotechnol*. 2016;7(3):1–9. doi:10.1088/2043-6262/7/3/035008
21. Ferrari AC. Raman spectroscopy of graphene and graphite: disorder, electron-phonon coupling, doping and nonadiabatic effects. *Solid State Commun*. 2007;143(1–2):47–57. doi:10.1016/j.ssc.2007.03.052
22. Yan J, Fan ZJ, Wei T, Qian WZ, Zhang ML, Wei F. Fast and reversible surface redox reaction of graphene-MnO2 composites as supercapacitor electrodes. *Carbon*. 2010;48(13):3825–3833. doi:10.1016/j.carbon.2010.06.047
23. Hu Z, Huang YD, Sun SF, et al. V[illegible]ble ligh[illegible]riven photodynamic anticancer activity of graphene [illegible]de/TiO2 hybr[illegible] *Carbon*. 2012;50(3):994–1004. doi:10.1016/j.carb[illegible]2011.10.002
24. Zhou Y, Bao QL, Tang [illegible]L, Zh[illegible] YL, Loh [illegible]P. Hydrothermal dehydration for the "g[illegible]n" reduction [illegible]exfol[illegible]ed graphene oxide to graphene and de[illegible]istration [illegible]tunable [illegible]al limiting properties. *Chem Mater*. 2009;[illegible]13):28[illegible]–2956. doi:10.1021/cm9006603
25. Peng XY, [illegible] X[illegible]iamond F[illegible] Lau KT. Synthesis of electroche[illegible]ally-reduced [illegible]raphen[illegible]oxide film with controllable size an[illegible]ness and its [illegible] supercapacitor. *Carbon*. 2011;49(11):3[illegible]88–349[illegible]oi:10.1016/j.carbon.2011.04.047
26. Loh KP, Bao Q[illegible]Eda G, Chhowalla M. Graphene oxide as [illegible]chemically tunable [illegible]latform for optical applications. *Nat Chem*. 2010;2(12):1015–1024. doi:10.1038/nchem.907
27. Chang YR, [illegible]ee HY, Chen K, et al. Mass production and dynamic imaging of [illegible]luorescent nanodiamonds. *Nat Nanotechnol*. 2008;3(5):284–28[illegible]doi:10.1038/nnano.2008.99
28. [illegible] Boisseaux P, Fernandez-Cruz ML, Navas JM. Internalization and cytotoxicity of graphene oxide and carboxyl graphene nanoplatelets in [illegible]human hepatocellular carcinoma cell line HepG2. *Part Fibre Toxicol*. 2013;10:27–48. doi:10.1186/1743-8977-10-27
29. Hong SC, Lee JH, Lee J, et al. Subtle cytotoxicity and genotoxicity differences in superparamagnetic iron oxide nanoparticles coated with various functional groups. *Int J Nanomed Nanotechnol*. 2011;6:3219–3231.
30. Mesarosova M, Kozics K, Babelova A, et al. The role of reactive oxygen species in the genotoxicity of surface-modified magnetite nanoparticles. *Toxicol Lett*. 2014;226(3):303–313. doi:10.1016/j.toxlet.2014.02.025
31. Buzea C, Pacheco II, Robbie K. Nanomaterials and nanoparticles: sources and toxicity. *Biointerphases*. 2007;2(4):MR17–MR71.
32. Koedrith P, Boonprasert R, Kwon JY, Kim I, Seo Y. Recent toxicological investigations of metal or metal oxide nanoparticles in mammalian models in vitro and in vivo: DNA damaging potential, and relevant physicochemical characteristics. *Mol Toxicol*. 2014;10(2):107–126. doi:10.1007/s13273-014-0013-z
33. Liu YY, Luo Y, Wu J, et al. Graphene oxide can induce in vitro and in vivo mutagenesis. *Sci Rep*. 2013;3:3469. doi:10.1038/srep03469
34. Akhavan O, Ghaderi E, Akhavan A. Size-dependent genotoxicity of graphene nanoplatelets in human stem cells. *Biomaterials*. 2012;33(32):8017–8025. doi:10.1016/j.biomaterials.2012.07.040
35. Jaworski S, Sawosz E, Grodzik M, et al. In vitro evaluation of the effects of graphene platelets on glioblastoma multiforme cells. *Int J Nanomed*. 2013;8:413–420.
36. Hinzmann M, Jaworski S, Kutwin M, et al. Nanoparticles containing allotropes of carbon have genotoxic effects on glioblastoma multiforme cells. *Int J Nanomed*. 2014;9:2409–2417.
37. Zhang G, Chang HC, Amatore C, Chen Y, Jiang H, Wang XM. Apoptosis induction and inhibition of drug resistant tumor growth in vivo involving daunorubicin-loaded graphene-gold composites. *J Mat Chem B*. 2013;1(4):493–499. doi:10.1039/C2TB00378C

38. Zhang Y, Ali SF, Dervishi E, et al. Cytotoxicity effects of graphene and single-wall carbon nanotubes in neural phaeochro -mocytoma-derived PC12 cells. *ACS Nano*. 2010;4(6):3181–3186. doi:10.1021/nn1007176
39. Zhao H. Extrinsic and Intrinsic Apoptosis Signal Pathway Review. In: Ntuli T, editor: Apoptosis and Medicine. London, UK: IntechOpen; 2012. doi: 10.5772/50129
40. Pistritto G, Trisciuoglio D, Ceci C, Garufi A, D'Orazi G. Apoptosis as anticancer mechanism: function and dysfunction of its modulators and targeted therapeutic strategies. *Aging-US*. 2016;8(4):603–619. doi:10.18632/aging.100934
41. Lao F, Chen L, Li W, et al. Fullerene nanoparticles selectively enter oxidation-damaged cerebral microvessel endothelial cells and inhibit JNK-related apoptosis. *ACS Nano*. 2009;3(11):3358–3368. doi:10.1021/nn900912n
42. Smith AM, Mancini MC, Nie S. Bioimaging: second window for in vivo imaging. *Nat Nano*. 2009;4(11):710–711. doi:10.1038/nnano.2009.326

Supplementary materials

Figure S1 HepG2 cell line incubated for 24 hours with 400 µg/mL of (**A**) graphene nanosheets, (**B**) magnetite nanoparticles, (**C**) G[illegible]agnet[illegible]nocomposite. Inverted microscopy (phase contrast, 40x).

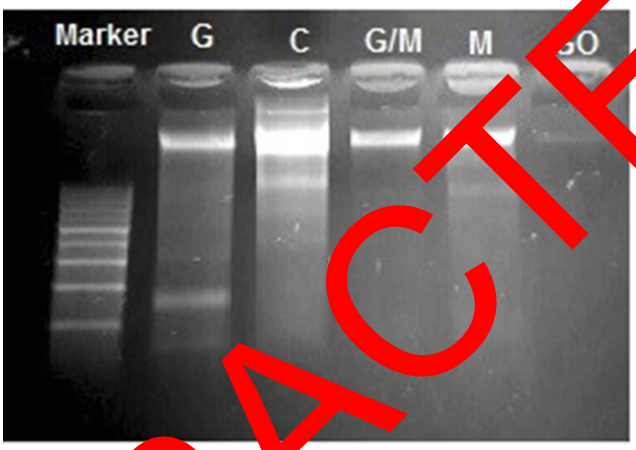

Figure S2 EB-stained gel electrophoresis of genomic D[illegible]x extracti[illegible] from unt[illegible]ted and treated HepG2 cell line with 400 µg/mL of prepared materials, Lane 1 Marker (ladder 100 bp), Lane2 G (HepG2 treated with graph[illegible]e), Lane 3 [illegible]ntrol (untre[illegible]ed HepG2), Lane 4G/M (HepG2 treated with graphene/magnetite), Lane 5 M (HepG2 treated with magnetite), and Lane 6 GO (HepG2 [illegible]reate[illegible]with [illegible]phene [illegible].

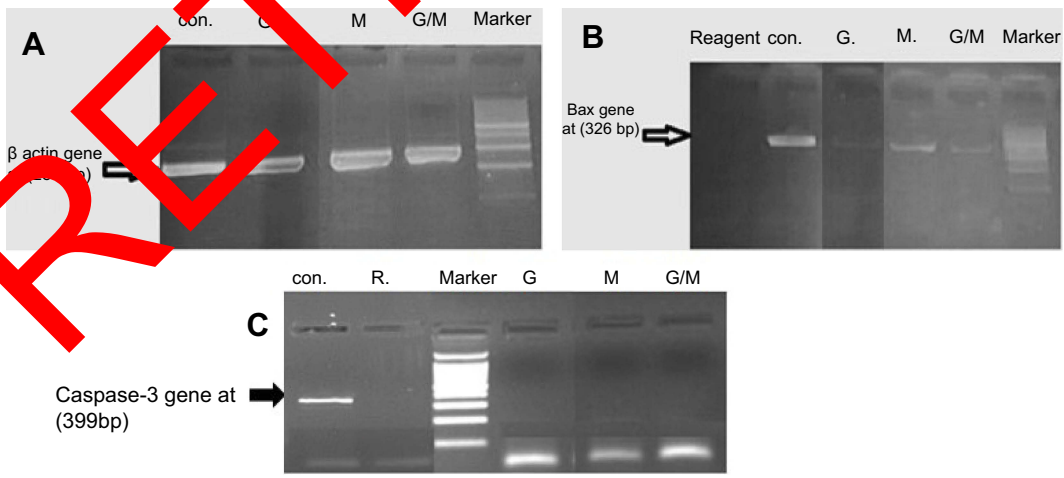

Figure S3 EB-stained gel electrophoresis of (**A**) genomic β-actin RNA genes Marker 100 pb (β-actin at 253 bp), (**B**) genomic Bax RNA genes Marker 100 pb (Bax at 326 bp), (**C**) genomic caspase-3 RNA genes (caspase-3 *at 399 bp)* from untreated and treated HepG2 cell line with 400 µg/mL of prepared materials, control (untreated HepG2), G (HepG2 treated with graphene), M (HepG2 treated with magnetite), G/M (HepG2 treated with graphene/magnetite), R (reagent) and ladder at Marker lane.